WILEY | Hindawi

Research Article

Enclosed Karst Depression Identification and Analysis for the Pumped Storage Power Station Reservoir Construction Using DEM

Yu Bo,[1,2] **Zhang Tao** [iD][2,3] **Zheng Kexun,**[1,2] **Zuo Shuangying,**[2,3] **Han Xiao,**[1] **Wang Senlin,**[1] **and Chen Shiwan**[2,3]

[1]*Power China Guiyang Engineering Corporation Limited, Guiyang 550081, China*
[2]*Key Laboratory of Karst Georesources and Environment, Ministry of Education, Guizhou University, Guiyang 500025, China*
[3]*College of Resources and Environment Engineering, Guizhou University, Guiyang 550025, China*

Correspondence should be addressed to Zhang Tao; gs.yltian22@gzu.edu.cn

An enclosed karst depression, a typical natural negative terrain, has the advantage of less engineering excavation when constructing a reservoir. In this study, the enclosed karst depression and its range identification technique have been developed. What is more, the geometric parameters and spatial distribution of enclosed karst depressions in Anlong County, Guizhou Province of China, have also been analyzed. Results show that (1) the focus statistic method and local terrain contour tree model were developed to identify enclosed karst depression and its range using regular grid DEM data with 12.5 m spatial resolution, which has been applied to enclosed karst depression identification in Anlong County. (2) 7262 independent and nested depressions with an average density of 3.7/km² were identified by using the proposed method. The effectiveness and reliability of the proposed model have been verified through comparative analysis and visual recognition comparison. (3) High-density depression areas (5.6 depressions/km²), medium-density depression areas (2.9 depressions/km²), and low-density depression areas (1.1 depressions/km²) were well classified through kernel density analysis. (4) The geometric parameters of enclosed karst depressions (area, perimeter, circularity, depth, elevation, slope, and volume) were all analyzed in the study area. In addition, an indicator called DCK (depression is caused by karstification) was proposed to evaluate the dissolution degree and karstification stage of the enclosed karst depression. Based on the DCK, we determined that around 2.7% of depressions were identified as middle-stage and suitable for reservoir construction with enough volume and good slope stability. The idea and method in this research could provide a technological support for the engineering utilization of enclosed karst depressions.

1. Introduction

An enclosed karst depression is a certain area of closed or semiclosed negative terrain basin formed by the dissolution of carbonate rocks in karst areas, and it is a typical type of karst landform. In southwest China, the karst area distribution is more than 500,000 km². Guizhou Province is located in the core area of this karst region, and the area of soluble rock accounts for 77% of the whole territorial area, in which karst peak-cluster depression is the main type of landform. The enclosed karst depression with natural negative terrain has good potential in the water reservoir, tailing reservoir,

and technology infrastructure for its good stability and less excavation [1–3]. Many researchers have studied the development, evolution, genesis, and classification of enclosed karst depression [4, 5], especially in recent years, some automatic detection methods and technologies on different types of karst depressions have been proposed [6–18], but there is a lack of research on the engineering utilization of enclosed karst depressions [19, 20].

Accurate recognition and range extraction of enclosed karst depression are the key issues for its engineering utilization. The enclosed karst depression extraction mainly depended on the field survey and sketching the depression
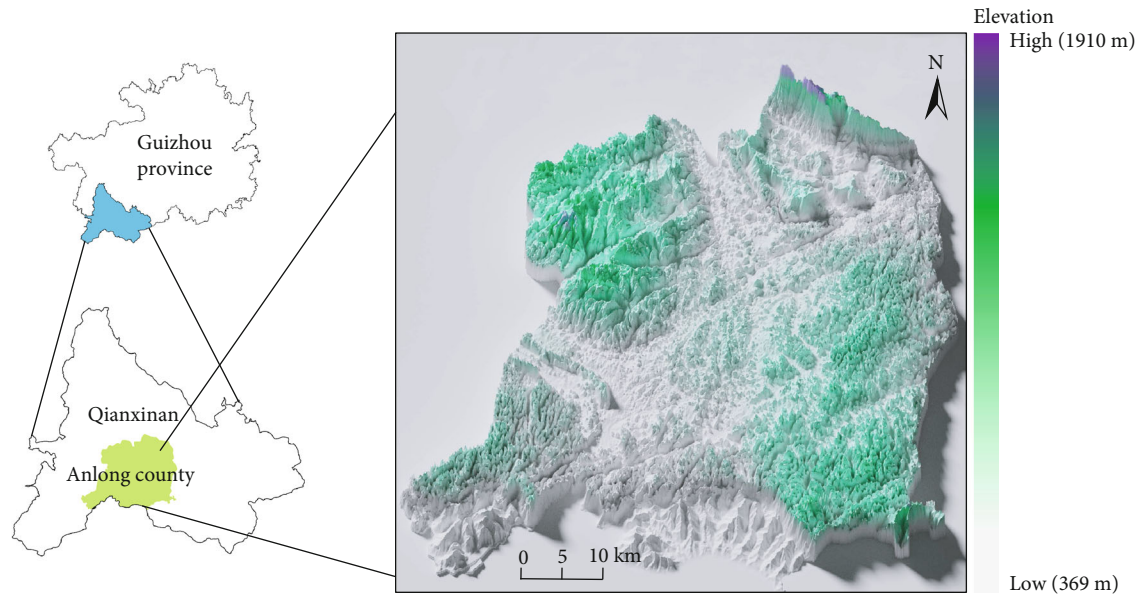
Figure 1: Geographical location and 3D terrain map of the study area.

outline manually using low-resolution topographic geomorphology maps in the last century, which was time-consuming and inefficient [21–23]. The work was improved by the application of digital elevation model (DEM) with high resolution [24, 25], which can well facilitate depression identification and evaluation [26], such as the sink-filling method [27, 28], saddle point method [29–32], and terrain contour tree method [33–36]. However, there are also many difficulties, for example, pseudo depressions, poor accuracy for saddle points, and identifying nested depressions are to be addressed [37]. Therefore, it is importance to improve the extraction technique of enclosed karst depression for the engineering development and utilization.

There were more studies on the utilization of karst depression in animal ecology, nature protection, geological tourism, geological relic protection, and geohazard prevention applications [38–43]. They have been studied quantitatively using spatial distribution parameters and morphological statistics [44–48]. With the improvement of DEM resolution in recent years, the recognition, characterization, and quantification of enclosed karst depressions have also been improved significantly. Hao et al. [49] and Yang [50] applied kernel function and kernel density to classify the spatial pattern through the depression density, which is reliable in discriminating the aggregation and similarity among geographical objects. Many researchers used indexes such as elevation, area, perimeter, depth, length, width, average diameter, aspect ratio, roundness, elongation, tensile length, and compactness hypsometric integral (HI), to characterize the closed depression morphology [51–56]. These parameters are easily to be obtained from the GIS platforms.

The enclosed karst depression is one of the important alternative sites for pumped storage power station reservoir and tailing reservoir [57]. Especially in the construction of pumped storage power station, enclosed karst depressions can be used as the upper reservoir, and nearby rivers or existing reservoirs as the water source of the lower reservoir. The lower water is pumped to the upper reservoir using the electric energy during the low power load and released into the lower reservoir to generate electricity during the peak power load [1]. Therefore, to develop effective and reliable identification and evaluation technique of depression is significant for engineering utilization. In this work, the enclosed karst depression extraction and evaluation parameters are studied and applied in the research area, which could provide some support for the resource utilization of depressions.

2. Research Area and Data Source

2.1. Geological Condition of the Research Area. As shown in Figure 1, the research area, Anlong County, is located on the north bank of the Nanpanjiang River, Guizhou Province of China. It goes through the transition zone from Yunnan-Guizhou Plateau to Guangxi hills, covering an area of $2237 \, km^2$, with the highest elevation of 1910 m, the lowest elevation of 369 m, and a height difference of about 1541 m (Figure 1). The whole river system belongs to the Pearl River Basin. The overall terrain presents a step-like shape and gradually descends from the middle mountain area in the west to the hilly basin valley in the east. The geomorphology of the research area is composited of the mountain, hill, basin, valley, peak cluster, peak forest, and karst depression. The underground river distributes throughout the whole area. The carbonate strata account for 84% of the whole area and the lithology is mainly thick-bedded dolomite. Due to the strong geotectonic movement in the geological history, its geological structure and geological environment are very complicated in Anlong County. With the crustal movement, lifting, denudation, and planation process, high karstic plateau mountains have been formed as the core distribution area of the karst geomorphic landscape in Guizhou.
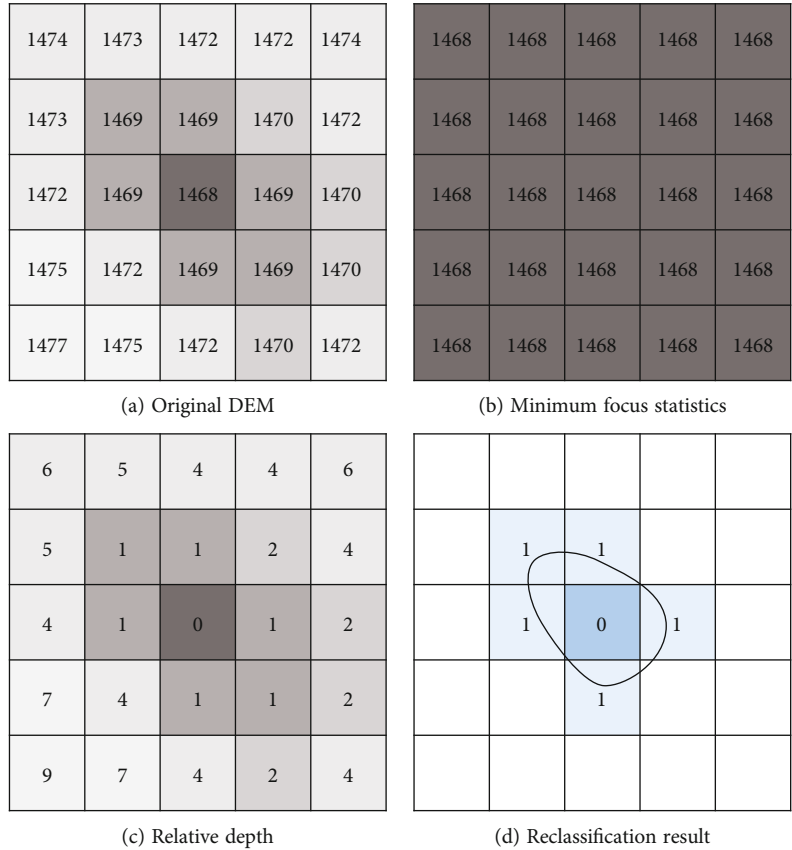
1474	1473	1472	1472	1474
1473	1469	1469	1470	1472
1472	1469	1468	1469	1470
1475	1472	1469	1469	1470
1477	1475	1472	1470	1472

(a) Original DEM

1468	1468	1468	1468	1468
1468	1468	1468	1468	1468
1468	1468	1468	1468	1468
1468	1468	1468	1468	1468
1468	1468	1468	1468	1468

(b) Minimum focus statistics

6	5	4	4	6
5	1	1	2	4
4	1	0	1	2
7	4	1	1	2
9	7	4	2	4

(c) Relative depth

	1	1		
	1	0	1	
		1		

(d) Reclassification result

Figure 2: The schematic diagram of valley bottom identification by focus statistics.

2.2. Data Source.

The topographic data used in this work comes from the DEM raster data with 12.5 m spatial resolution, which was mapped by Japan's ALOS earth observation satellite and was acquired from the website https://urs.earthdata.nasa.gov. The downloaded data of the research area would be imported into ArcGIS 10.8 software and preprocessed with geometric correction, joint coating, and vector cutting to establish regular grids of DEM, providing the data foundation for the extraction of the depressions.

3. Methods

3.1. Automatic Extraction of Enclosed Karst Depressions

3.1.1. Depression Identification Using Neighborhood Analysis.

Regular grids of DEM divide the surface topography into individual grid cells which store the surface elevation in the form of pixel data. Using the focus statistics tool of ArcGIS10.8 software, elevation statistics of the grid data in the specified neighborhood window are calculated by the neighborhood analysis tool. The algorithm will iterate through every pixel to be processed during execution, and the pixel value in the neighborhood window is allowed to overlap with other neighborhood windows, so the same pixel can be included in different neighborhood windows.

As shown in Figure 2(a), in the studied rectangular with a specified length and width, the algorithm will process all the pixels in the rectangular neighborhood and scan each grid pixel in the terrain region in an ergodic style. The elevation of the central pixel is used to compare with its surrounding rectangular neighborhood. If the value of all neighboring pixels is higher than that of the central pixels, the statistical data will be the minimum value, and the elevation value of the central pixel would be assigned to all neighboring pixels. The generated new DEM data are shown in Figure 2(b).

As shown in Figure 2(c), the difference between the original DEM data and the new DEM data is calculated by neighborhood analysis which is used to obtain the elevation difference of each pixel relative to the minimum value in the neighborhood window. Then the depression is reclassified according to the relative depth, whose value is greater than 1 will be assigned to NODATA and the segmentation threshold is set to 1, so as to identify the bottom of the depression, as shown in Figure 2(d). The bottom of an enclosed karst depression can be identified using this method [58].

3.1.2. Depression Boundary Identification.

The enclosed karst depression is a kind of concave catchment terrain, which can collect the surrounding water flow to reach overflow elevation [26, 59], and the corresponding elevation is called the spill elevation of the depression [34]. Once the spill elevation is reached, the water level will reach the maximum. The closed surface is called as the maximum contour surface of the depression (Figure 3(a)). If the two more adjacent

(a) Single depression
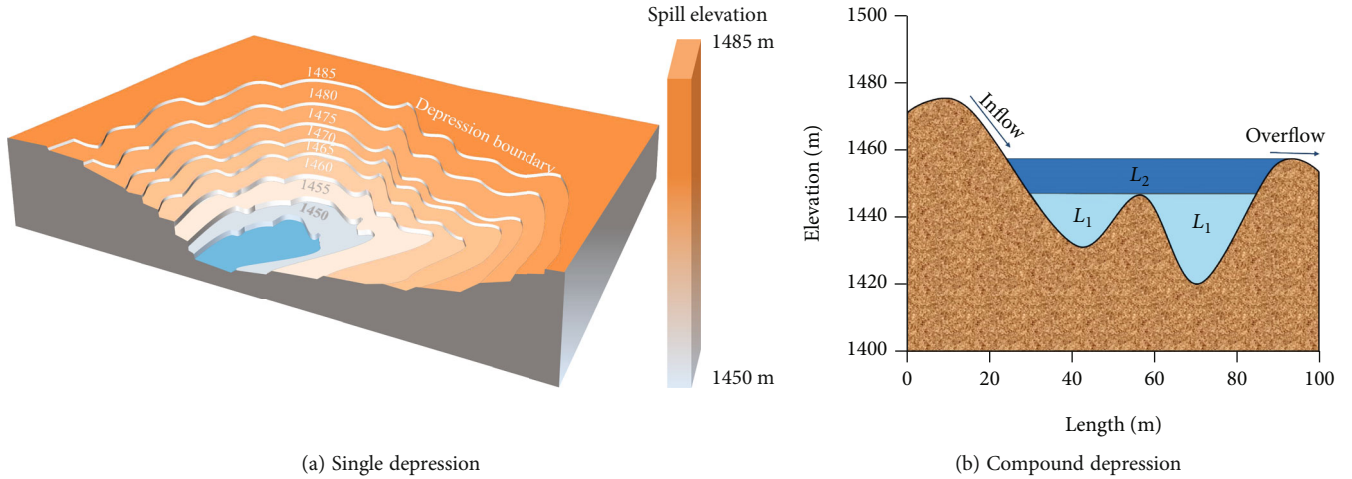
(b) Compound depression

FIGURE 3: Spillover elevation map of depression.

depressions have the same spill elevation, these adjacent depressions can be merged into a compound depression (Figure 3(b)). Thus, after the identification of the depression bottom, the spill elevation is used to fill the depressions to obtain the boundary of the depressions.

3.1.3. Terrain Contour Tree Model of Compound Depression.

The enclosed karst depression can be identified and its range can be delineated for a single depression by the above method. However, delineating the range of compound depression in the specified area requires the terrain contour tree algorithm, which was proposed by Kweon and Kanade (1994) as a graph theory method to represent the topological relations of hierarchical contours. Wu et al. proposed the global contour tree method and local contour tree method to judge the inclusion relations between closed contours to build the region expansion algorithm method, which was widely used in surface morphology analysis and geomorphic type recognition [21, 60]. In this method, the establishment of the tree is controlled by nodes and edges. Nodes represent the regions contained in each rank of closed contour, and the topological relations between adjacent nodes represent edges. The initial closed contour line in the depression valley is set as the seed node, and the contour tree is gradually simplified according to the adjacency or inclusion relation in the nested relation of contour line. Finally, a complete local contour tree is generated.

Figure 4 shows the local contour tree construction process of a nested depression. Three closed contours L_1, L_3, and L_5 are seed nodes, which are composed of the first-rank contours at depression valley. Then the contour is increased from seed nodes with the specified contour interval step by step. For each step, it is necessary to judge whether the increased contour contains more seed nodes. If more seed nodes are encircled in the increased contour, a node of higher rank will need to be defined which could cover the range of the contour line delineated. As shown in Figure 4, L_1 and L_2 are the nodes with the same rank, while L_4 contains two seed nodes L_2 and L_3, so the node L_4 is at the highest rank. All contours are traversed successively until the boundary node L_6 of the depression is identified. The con-

tour tree model is simplified by remaining the seed nodes and removing the superfluous nodes.

3.2. The Calculation of Spatial Characteristics of Enclosed Karst Depressions

3.2.1. Fundamental Spatial Characteristic.

Enclosed karst depressions always characterize as varied morphology and uneven spatial distribution. It is important to characterize the morphology of the depression in the field to reflect its feature; however, the field survey is time-consuming and laborious. Many GIS tools could facilitate the geometric parameter extraction of the enclosed karst depression, including area (S), circumference (T), depth (h), slope (p), elevation (H), and volume (V). The area and circumference of the depression are defined as the plane area and side length of the closed contour corresponding to the maximum spill elevation. The depth is defined as the maximum vertical distance between the maximum spill elevation and the depression bottom, and the slope is obtained by statistical averages within the range of depressions.

The capacity of reservoirs is also an important geometric parameter for an enclosed karst depression, which reflect the volume of an enclosed karst depression. The volume calculation requires to accurately extracting the boundary and depth, which were often ignored by previous studies [12, 61]. In this work, the capacity of reservoir is defined as the volume of a closed body enclosed by circles of contour lines between the depression bottom and the maximum spill elevation plane. The DEM data of each depression is extracted and formed into a closed contour of the maximum spill elevation. In the volume calculation, the volume of the depression is divided into many prismoids whose bottom edge length D is 12.5 m, and the height is the depth of the relative spill elevation plane. Then the total volume is obtained by summing all the quadrangular prismoidal units in the range of the depression. The volume calculation formula for a quadrangular prismoidal unit is written as follows:

$$V(h_i) = D^2 \times (H - h_i), \tag{1}$$

(a) Closed depression contour tree   (b) Contour tree   (c) Simplified contour tree
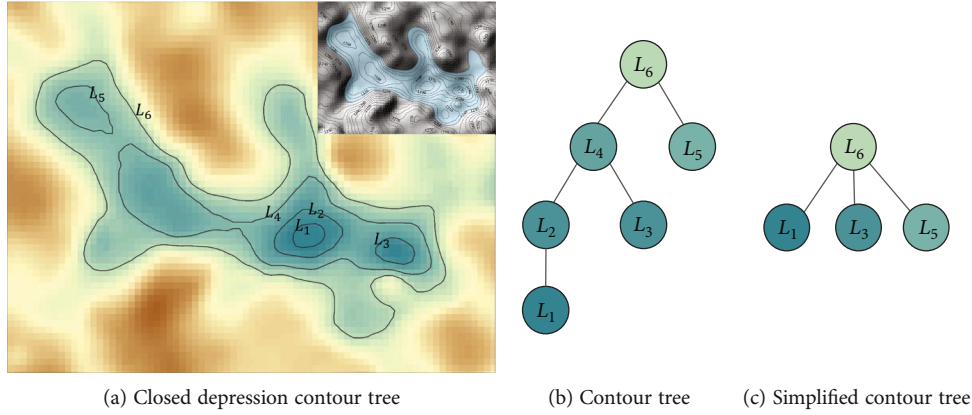
FIGURE 4: Closed contour lines and corresponding contour tree structure in depressions.

where H is the maximum spill elevation value of the depression, h_i is the relative depth, and D is the edge length of regular grid DEM.

The total volume of an enclosed karst depression is

$$V = V(h_1) + V(h_2) + \cdots + V(h_n) = \sum_{i=1}^{n} V(h_i). \qquad (2)$$

3.2.2. K Function and Kernel Density. The spatial pattern analysis of depressions is carried out by using the K function [62], and the kernel density calculates spatial distribution patterns mainly. K function is centered on a single point element as follows [50]:

$$K(d) = \frac{A}{n^2} \sum_i \sum_{i \neq j} I(d_{ij}), \qquad (3)$$

where A is the area of research region. d is the spatial distance. n is the total number of geographic objects. $I(d_{ij})$ is the number of geographical objects within the circle whose center is i and radius is d_j (the j-grade). During the calculation, the initial distance is set to 0, the increasing distance interval is 2 km, and the maximum distance is 40 km. Finally, both the curve from the observed value and the curve from expected value are generated. When the observed value is higher than the expected value, it indicates that the point data has a high degree of aggregation. On the contrary, when the observed value is smaller than the expected value, it indicates that the point data is distributed discretely, and the optimal spatial clustering analysis distance is calculated by the K function.

The spatial density difference can be characterized by using the kernel density, which generates a smooth spatial trend surface based on the density value of point data within a certain range. The trend chart of density-spatial distribution is determined by setting the search radius. The default search radius is calculated as follows [50]:

$$R = 0.9 * \min\left(SD, \sqrt{\frac{1}{\ln(2)}} * D_m\right) * n^{-0.2}, \qquad (4)$$

where SD is the standard distance between point data, D_m is the median distance between point data, and n is the total number of points.

3.2.3. The Indicator of DCK. In order to evaluate the relative dissolution degree and difference of enclosed karst depressions in the same area, the index DCK generated by karst process was proposed. The original carbonate rock mass before karstization is simplified into a prismoid geometry, as shown in Figure 5(a), and the bottom face is defined as the plane surrounded by the current enclosed karst depression boundaries (that is, the maximum spill elevation surface). The height is regarded as the maximum depth of the depression, so that the volume of the prismoid block can be equivalent to the initial volume ($V_0 = S \times h$). The volume of enclosed karst depression is the loss of surface karstification, and DCK is defined as the ratio of the depression volume (V) to the initial volume (V_0) (Figure 5).

$$\mathrm{DCD} = \frac{V}{V_0} = \frac{V}{S \times h}, \qquad (5)$$

where V is the volume of single enclosed karst depression. S is the area of the maximum spill elevation plane. h is the maximum depth of enclosed karst depressions.

4. Results

4.1. Depression Extraction Results and Precision Analysis. The bottom and range of an enclosed karst depression were identified by focus statistics and spill elevation, and then the boundaries of nested depressions were delineated by the local terrain contour tree method. On ArcGIS 10.8, 11709 depressions and sink region were identified in the research area (2237 km^2). 7262 independent and nested depressions were obtained by a local contour tree method (Figure 6). The average density of enclosed karst depressions was 3.7/ km^2 after excluding all nonconforming pseudo depressions.

To verify the accuracy of the algorithm, a small area in the southwest of the research area was selected for comparative analysis as a sample area, mainly by comparing with the previous research results and visual identification. In the research area, Yan et al. [18] counted 475 depressions
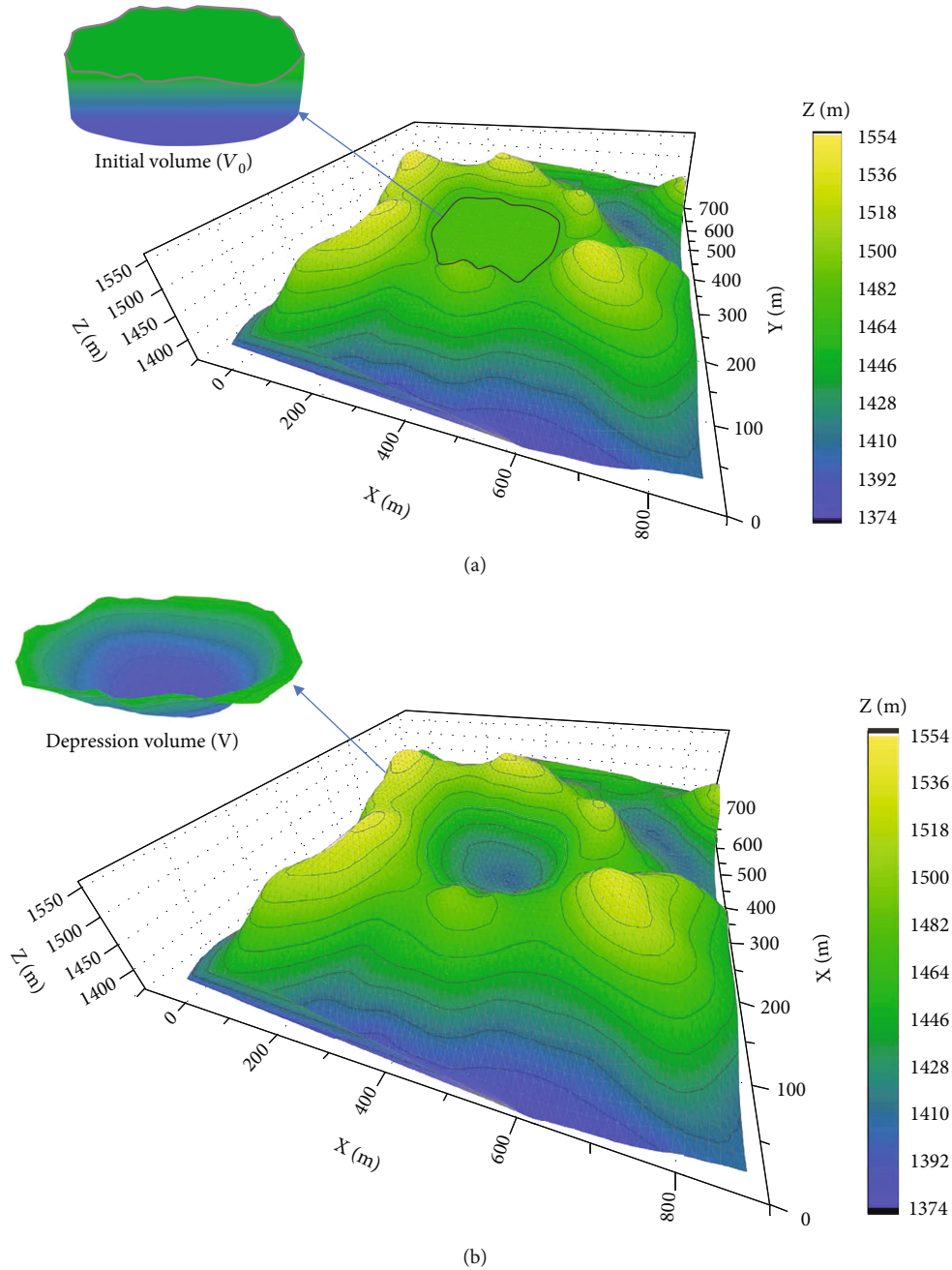
(a)

(b)

FIGURE 5: Schematic diagram of DCK concept. (a) Before the formation of enclosed karst depression. (b) After the formation of enclosed karst depression.

through satellite data, topographic map, and field reconnaissance, and extracted 391 depressions based on Landsat 8 remote sense images, with an extraction accuracy of less than 85%. In this work, 521 enclosed karst depressions were extracted in the same area (Figure 7(a)). In addition, the extracted results were imported into Google Earth to increase the resulting visibility (Figure 7(b)). The results showed that the depression identification was of high accuracy, and the method can extract the enclosed karst depressions with small area and high vegetation cover, which demonstrated the effectiveness of this algorithm.

4.2. The Spatial Pattern Characteristics of Enclosed Karst Depressions. The spatial pattern analysis of 7262 enclosed karst depressions extracted from the research area (2237 km^2) was carried out. The results showed that the enclosed karst depressions were characterized as spatial aggregation in the distance range of 0~22 km and converted to discrete distributions when the distance was larger than 22 km (Figure 8(a)). The search radius L was determined as 7 km by analyzing the K function. As shown in Figure 8(b), the spatial distribution of enclosed karst depressions was calculated by the kernel density analysis method.
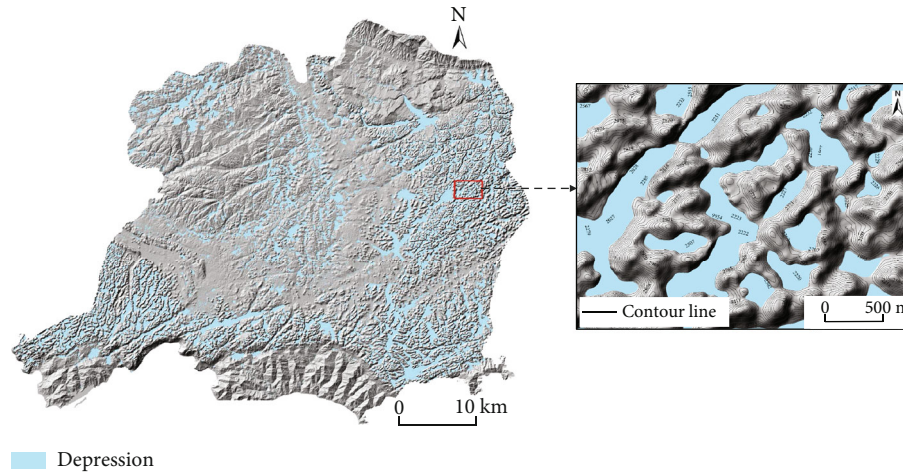
FIGURE 6: Extraction results of enclosed karst depression in research area.
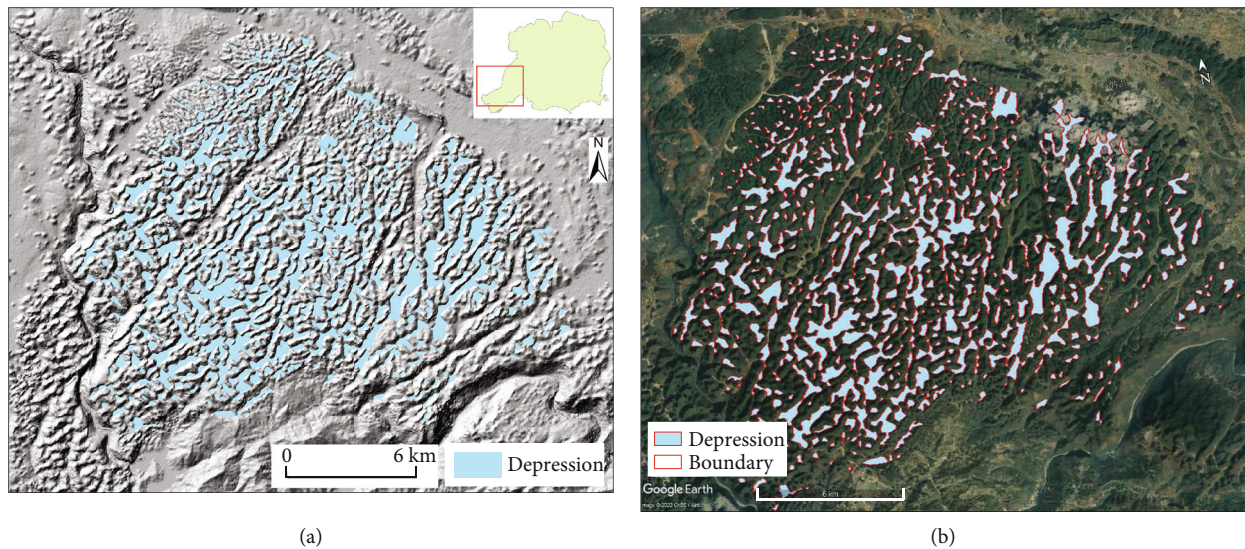

(a)

(b)

FIGURE 7: Extraction results of enclosed karst depression. (a) Automatic extraction results of enclosed karst depression in sample area. (b) Extracted results for visual evaluation.

The research area was divided into three grades according to the depression density from high to low: high-density area (L_1), medium-density area (L_2), and low-density area (L_3). The morphological parameters of three kinds of depressions with different densities are shown in Table 1. The average density of depressions in high-density area is 5.3 depressions/km^2 with the area of 288 km^2, which are located in the northeast and middle of the area. The medium-density area is the continuation of the high-density area and is widely distributed, with an average density of 2.9 depressions/km^2. While the low-density area is mainly distributed in the steep slope zone, the density of depressions is merely 1.1 depressions/km^2. The average area, elevation, depth, and slope of three kinds of depressions are also listed in Table 1.

4.3. Plane Characteristics of Enclosed Karst Depressions. To systematically and scientifically screen out good enclosed karst depression for engineering utilization, it is necessary to characterize the geometry of enclosed karst depressions accurately using some rational parameters. The results of morphologically characteristic parameters obtained from enclosed karst depressions extracted automatically are shown in Table 2.

The morphological parameters of enclosed karst depressions are shown in Figure 9. There were obvious differences and large span of parameters. The maximum area of depressions is 9.32 km^2, while the minimum area is only 0.0015 km^2, and the average area is 0.065 km^2. Depressions with the area greater than 0.1 km^2 account for 9.11%, and the area of depressions is concentrated between 0.003 km^2 and 0.01 km^2 (41.58%), as shown in Figure 9(a). According to the Jenks Natural Breaks Classification Method [63], these depressions can be divided into five categories: ultrasmall (0~0.14 km^2), small (0.14~0.57 km^2), medium

(a) *K* function analysis result
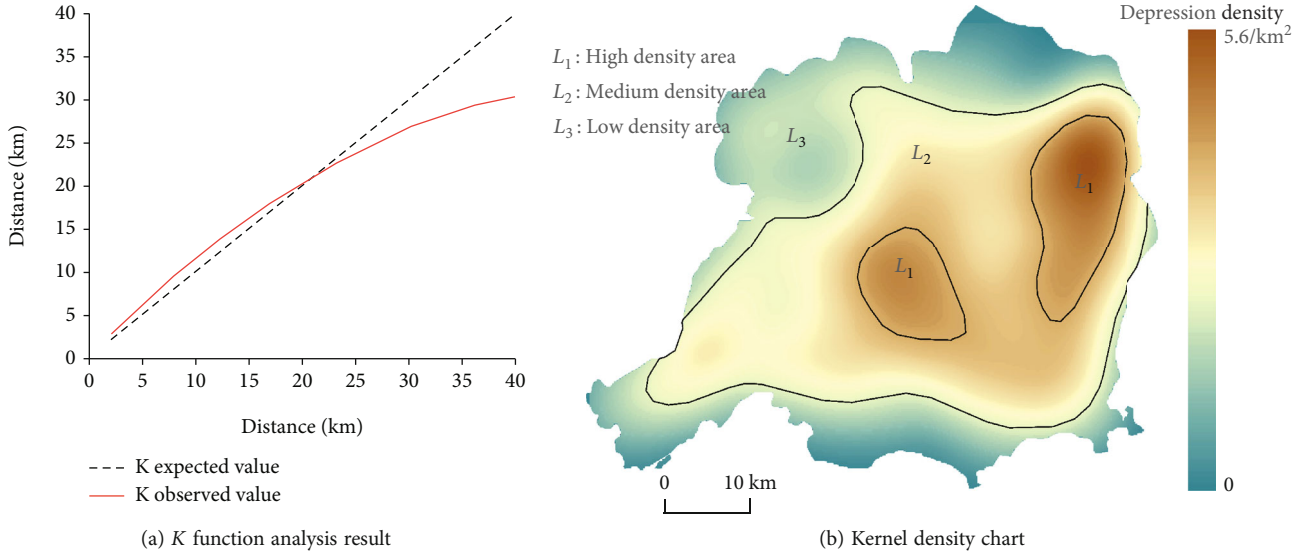
(b) Kernel density chart

Figure 8: *K* function analysis and nuclear density diagram.

Table 1: Morphological parameters of depressions in different density areas.

Region	Average density of depression (km^{-2})	Average area of depressions (km^2)	Elevation of depression valley (m)	Average depth (m)	Average slope (°)
High-density area	5.6	0.069	971-1440	20	28
Medium-density area	2.9	0.089	1008-1548	20	27
Low-density area	1.1	0.064	378-1645	18	26

Table 2: Statistical parameters of enclosed karst depressions in the study area.

Index	Area (m^2)	Perimeter (m)	Depth (m)	Slope (°)	Altitude (m)	Volume (m^3)	DCK
Minimum	1538.63	63.33	1.00	1.15	378.00	39.01	0.02
Maximum	9 320 584.21	87825.19	328.00	77.17	1684.00	3 122 060 632	0.98
Mean	64633.55	733.25	15.79	17.54	1239.93	5633973.59	0.15
Q1	4796.51	179.94	4.00	6.51	1182.00	1092.32	0.06
Q2	9579.46	300.33	7.00	11.98	1260.00	7158.59	0.12
Q3	28756.60	633.56	17.00	23.79	1343.00	82522.07	0.19

Note: Q1 is the first quartile and is equal to 25% of all values in the sample in ascending order. Q2 is the second quartile and is equal to 50% of all values in the sample in ascending order. Q3 is the third quartile and is equal to 75% of all values in the sample in ascending order.

(0.57~1.81 km^2), large (1.81~4.25 km^2), and super large (>4.25 km^2).

Generally, the perimeter is closely related to the area of a depression which increases with the increase of the depression area (Figure 9(b)). The parameter circularity *C* describes the roundness degree of depressions as follows [64]:

$$C = \frac{4\pi S}{T^2},\qquad(6)$$

where *C* is the measured value of circularity. *S* and *T* are the area and perimeter of single depression. The shape is closer to a circle as the *C* value is closer to 1, while the shape is narrower with the decreasing of the *C* value.

As shown in Figure 9(c), the majority of depressions (75%) were near round with the value of circularity in the range of 0.7~1.0, which indicated that the karstification of the research area is strong.

Figure 9(d) shows the depth distribution of enclosed karst depressions. The maximum depth of depressions is 328 m, and the average depth is 15.79 m. The depth of depressions is mainly concentrated between 4 m and 15 m, accounting for 72.38%. The most of the depressions are dominated by general depth (≤299 m), according to the classification of depth rank [65].
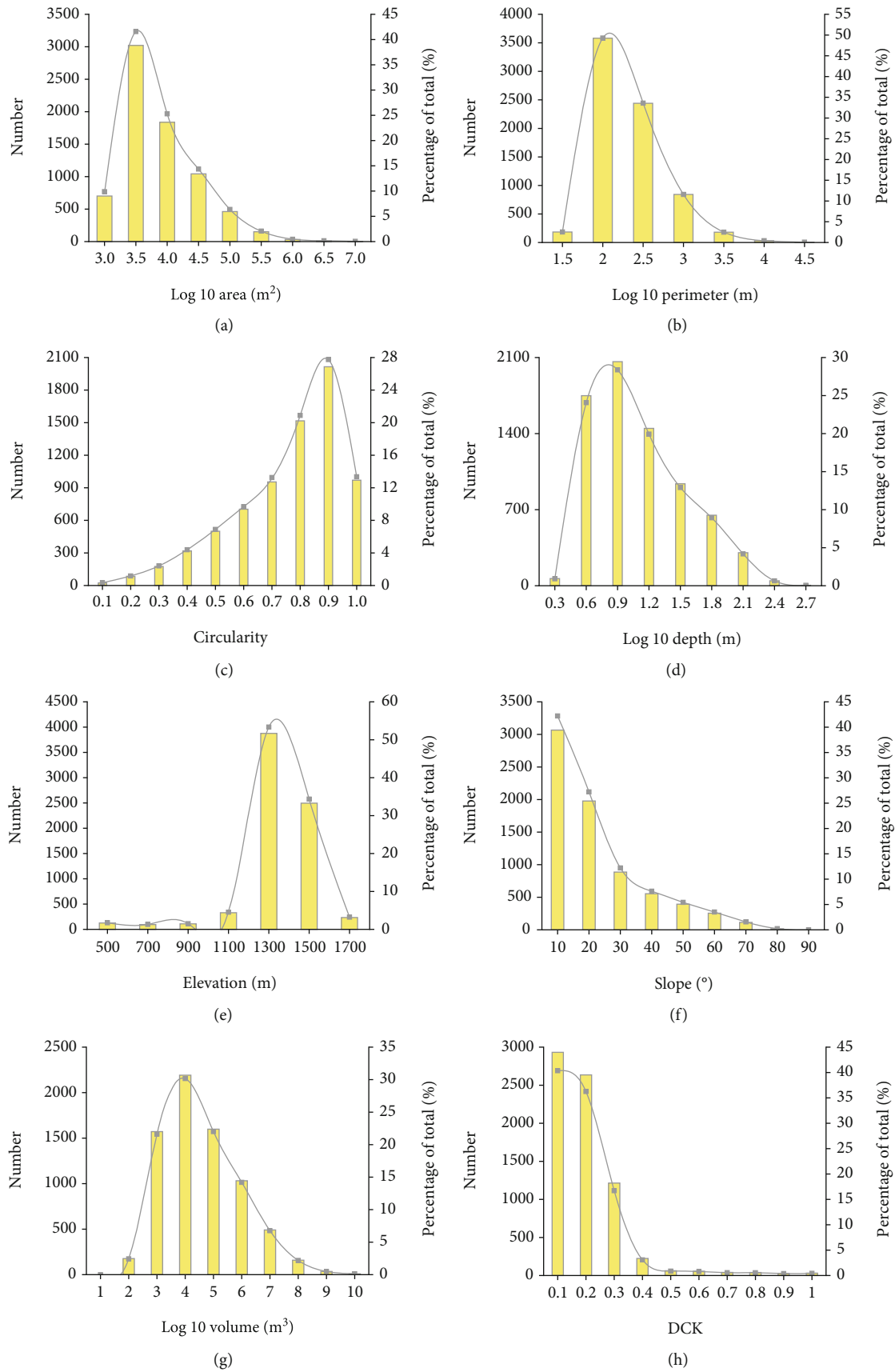
FIGURE 9: Histogram of morphological parameters of enclosed karst depression in research area. (a) Area. (b) Perimeter. (c) Circularity. (d) Depth. (e) Elevation. (f) Slope. (g) Volume. (h) DCK.

TABLE 3: development stage division of enclosed karst depression according to *DCK*.

Stage	DCK	Number of depressions	Proportion (%)	Suitable for reservoir or not
Juvenile stage	<0.15	4483	61.73	No
Youth stage	0.15~0.36	2477	34.11	No
Middle stage	0.36~0.68	196	2.70	Yes
Old stage	>0.68	106	1.46	No

In addition, the maximum altitude is 1910 m in the research area, the maximum elevation of the extracted depression valley is 1684 m, and the average elevation is 1239.93 m. What is more, the elevation of depressions concentrates in the elevation range of 1100 m~1500 m (Figure 9(e)), accounting for 87.71%, which illustrated that the depressions are mainly distributed in high gullies and in ridge enclosures, where the height difference is large.

Figure 9(f) shows the slope distribution of enclosed karst depressions. The maximum slope of depressions is 77°, with an average slope of 17.54°, and the slope of many depressions (42.21%) is less than 10°. The slope is mainly concentrated between 0° and 10° (gentle slope) and 10° and 20° (steep-slope) [66]. The density of depressions gradually decreases with the increase of slope, which reflects that the areas with larger slope are less developed due to the rapid discharge of surface water and weak infiltration capacity.

4.4. The Spatial Morphological Characteristics of Enclosed Karst Depressions. In previous researches, the volume of depressions was calculated approximately by using cone volume, which caused remarkable errors in volume calculation of the enclosed karst depression. In this work, the volume of depressions was calculated based on DEM with a 12.5 m resolution. This method embodied the real spatial morphological characteristics of depressions to a great extent. The volume of extracted enclosed karst depressions is concentrated between $1.0 \times 10^4 \, m^3$ and $1.0 \times 10^6 \, m^3$, accounting for 73.81%. (Figure 9(g)).

Enclosed karst depressions are controlled by the joints and fissures in different directions in carbonate rock strata during the early stage and gradually dissolved or corroded to form sink. With the crustal movement and rock dissolution, the joints and fissures expanded continuously, and the depressions deepened and widened. Finally, the negative terrain with different volumes formed gradually. So, through the analysis and evaluation of DCK of enclosed karst depressions, the development degree and difference of the depressions within the range of relatively consistent geological conditions can be spatially characterized. Meanwhile, DCK can reflect the availability degree of pumped storage power station reservoirs in the enclosed karst depressions.

Based on the statistics and analysis of the DCK value of a large number of enclosed karst depressions in this area, the relationship between the DCK and the karstification stage (juvenile stage, youth stage, middle stage, and old stage) was established according to the classical karst geomorphological theory, as shown in Table 3. The dissolution degree of an enclosed karst depression increases, and the excavation engineering quantity for a reservoir construction is smaller with the increasing DCK value. For the depression with a small DCK value, the karst development is in the early stage, and dam building work will be large due to the poor closure. The number of depressions with DCK less than 0.36 accounts for 95.84%, and the average value is 0.15, which are in the juvenile and youth stage of karst development. 2.70% of depressions are in middle age and have large dissolution space and better stability in slope, which can be built for reservoir development and utilization. Only 1.46% of depressions are in the old stage, whose slopes are too steep and not suitable for engineering application, as seen in Figure 9(h).

5. Discussion

The abundant enclosed karst depression in the research area has been widely recognized [67]. Although they are urgently needed to play an important role in plant protection, tourism development, and land use, they have not been fully identified and quantified due to the constraints of demand. This work focuses on extracting enclosed karst depressions by the local contour tree method based on DEM data and measuring the spatial characteristics of enclosed karst depressions in a GIS environment. This is an effective method for establishing an enclosed karst depressions (including sinkholes, dolines, and other negative terrain) database, which has been recognized and tested by more people [21, 68]. Compared with other extraction methods [18], the number of enclosed karst depressions extracted by the local contour tree method in the research area increased by 25%, and this result was also well visually verified in the latest satellite images on Google Earth (Figure 7(b)). At the same time, although many studies related to the identification of enclosed karst depressions are quoted in this work, this study pays more attention to delineating the actual boundary of enclosed karst depressions, which will provide a more accurate scope for the engineering application of enclosed karst depressions. However, in the extracted list of enclosed karst depressions, there are continuous flat areas and river valley trunk lines caused by the limitation of DEM contour, and the same situation also appears in Wu et al. [21] and Shaw-Faulkner et al. [69]. As suggested by Wu et al. [21], the number of pseudo-depressions caused by DEM errors can be reduced by setting surface area and depth thresholds.

There are great differences in the spatial characteristics of the enclosed karst depressions in the study area. For example, the average density of enclosed karst depressions in high-density areas is $5.3 \, km^{-2}$, while the average density in low-density areas is only $1.1 \, km^{-2}$. This phenomenon also

exists in Shilin County, Yunnan Province [4]. These two research areas are located in the core areas of karst development in southwest China and have complex stratigraphic composition, climatic conditions, and elevation differences, which are the main reasons for their spatial characteristics differences. From the actual situation, this is the result of different geomorphic evolution stages. For enclosed karst depressions in the juvenile and mature stages, the area is small and the density is generally large. When the depressions develop to the old stage, the depressions appear merging and nesting, showing the characteristics of large volume and wide area. In this work, the geometric parameters of other enclosed karst depressions were also measured, including circumference, depth, slope, and elevation. Parise et al. [70] pointed out that the measurement of geometric parameters is important data for the construction of enclosed karst depressions, and such information is helpful for the evaluation of engineering construction and disaster analysis of enclosed karst depressions [71].

Most notably, in previous studies [36], the measurement of morphological characteristics of enclosed karst depressions was mainly for geomorphic classification, and they focused on the selection of the most basic morphological indicators (such as elevation, slope, and area). Although these indicators can distinguish different geomorphic features to a certain extent, they fail to provide more detailed information on the engineering development of enclosed karst depressions. In contrast, an important aim of this study is to identify enclosed karst depressions and carry out reservoir construction for pumped storage power stations. Therefore, there is a bias in the selection of the spatial characteristics of the enclosed karst depression in this work. For example, the volume of depressions was selected in this study because it can directly reflect the water storage capacity of enclosed karst depressions, and the volume calculation requires accurate extraction of boundaries and depths, which are often ignored in previous studies [12, 61]. In general, this work is aimed at providing basic data for the development of important mountain resources in karst areas by extracting enclosed karst depressions and measuring spatial characteristics.

6. Conclusion

Enclosed karst depression is characterized as typical natural negative terrain, which has the advantage in less engineering excavation for the pumped storage power station reservoir construction. In this work, the enclosed karst depression and its range identification technique have been developed. And the geometric parameters and spatial distribution of enclosed karst depressions in Anlong County were analyzed.

(1) The focus statistics method and local terrain contour tree model were developed to identify enclosed karst depression and delineate its range using regular grid DEM data with 12.5 m spatial resolution. 7262 independent and nested depressions were identified using the proposed method, with an average density of 3.7/km^2. Through comparative analysis and visual recognition comparison, the proposed method was proven to be effective and reliable

(2) The enclosed karst depressions in the research area are characterized by uneven spatial distributions and different morphologies. There existed spatial aggregation characteristics in the range of 0~22 km and appeared discrete distribution outside the range of 22 km using the K function evaluation method. Meanwhile, high-density depression area (5.6 depressions/km^2), medium-density depression area (2.9 depressions/km^2), and low-density depression area (1.1 depressions/km^2) were classified using kernel density analysis

(3) Geometric parameters of enclosed karst depressions (area, perimeter, circularity, depth, elevation, slope, and volume) were analyzed in the research area. In addition, a new indicator, DCK (depression is caused by karstification), was proposed to evaluate the dissolution degree of the enclosed karst depression. The DCK value was used to evaluate the karstification stage of the enclosed karst depression, and 2.7% of the depressions were identified as middle stage and suitable for reservoir construction with enough volume and good slope stability

Nomenclature

K: Aggregation degree (-)
ρ: Density (number·km^{-2})
S: Area (m^2)
T: Circumference (-)
H: Depth (m)
P: Slope (°)
h: Altitude (m)
V: Volume (m^3)
DCK: Depression is caused by karstification.

Data Availability

The data presented in this study are available on request from the corresponding author.

Conflicts of Interest

No potential conflict of interest was reported by the author(s).

Authors' Contributions

Conceptualization was done by Yu Bo. Methodology was performed by Zhang Tao, Yu Bo, Zheng Kexun, Wang Senlin, and Han Xiao; Software was handled by Zhang Tao. The provision of the experimental data was done by Zhang Tao and Zuo Shuangying. Verification and validation were assigned to Zhang Tao and Zhengkexun. The investigation was performed by Z.L. Writing which includes the original draft preparation was assigned to Zhang Tao. Writing which includes review and editing was assigned to Chen

Shiwan, Wang Senlin, and Han Xiao. The visualization was done by Zhang Tao. Supervision was performed by Zuo Shuangying. All authors have read and agreed to the published version of the manuscript.

Acknowledgments

References

[1] A. Rogeau, R. Girard, and G. Kariniotakis, "A generic GIS-based method for small pumped hydro energy storage (PHES) potential evaluation at large scale," *Applied Energy*, vol. 197, pp. 241–253, 2017.

[2] Z. P. Shen, H. Wang, B. Wu, and J. Y. Fu, "Drainage countermeasures of karst depression at FAST platform," *Water Conservancy and Hydropower Technology*, vol. 47, no. 4, pp. 43–47, 2016.

[3] R. Zhao, Q. Zhang, and M. Xu, "Study on seepage in complex karst reservoir area based on numerical simulation," *South-to-North Water Diversion and Water Technology*, vol. 14, no. 3, pp. 150–155, 2016.

[4] Z. Q. Ding, X. Y. Yu, X. Gao, and Y. H. Li, "Study on spatial distribution characteristics and influencing factors of karst depression in Shilin County, Yunnan Province," *Carsologica Sinica*, vol. 38, no. 3, pp. 325–335, 2019.

[5] Z. Q. Ding, P. Wang, and Y. Li, "Study of dynamic mechanism of karst geomorphology evolution based on area-elevation integral value," *Quaternary Research*, vol. 41, no. 6, pp. 1546–1557, 2021.

[6] J. Obu and T. Podobnikar, "Algorithm for karst depression recognition using digital terrain models," *Geodetski Vestnik*, vol. 57, no. 2, pp. 260–270, 2013.

[7] M. Kobal, I. Bertoncelj, F. Pirotti, and L. Kutnar, "Lidar processing for defining sinkhole characteristics under dense forest cover: a case study in the dinaric mountains," *International Archives of the Photogrammetry, Remote Sensing & Spatial Information Sciences*, vol. XL-7, pp. 113–118, 2014.

[8] C. Bauer, "Analysis of dolines using multiple methods applied to airborne laser scanning data," *Geomorphology*, vol. 250, pp. 78–88, 2015.

[9] M. Kobal, I. Bertoncelj, F. Pirotti, I. Dakskobler, and L. Kutnar, "Using lidar data to analyse sinkhole characteristics relevant for understory vegetation under forest cover—case study of a high karst area in the dinaric mountains," *PLoS One*, vol. 10, no. 3, article e0122070, 2015.

[10] T. Telbisz, T. Látos, M. Deák, B. Székely, Z. Koma, and T. Standovár, "The advantage of lidar digital terrain models in doline morphometry compared to topographic map based datasets—Aggtelek karst (Hungary) as an example," *Acta Carsologica*, vol. 45, no. 1, pp. 5–18, 2016.

[11] J. Hofierka, M. Gallay, P. Bandura, and J. Šašak, "Identification of karst sinkholes in a forested karst landscape using airborne laser scanning data and water flow analysis," *Geomorphology*, vol. 308, pp. 265–277, 2018.

[12] T. Verbovšek and L. Gabor, "Morphometric properties of dolines in Matarsko podolje, SW Slovenia," *Environmental Earth Sciences*, vol. 78, no. 14, pp. 1–16, 2019.

[13] D. H. Doctor, J. M. Jones, N. J. Wood, J. T. Falgout, and N. I. Rapstine, "Progress toward a preliminary karst depression density map for the conterminous United States," in *Proceedings Of The 16th Multidisciplinary Conference On Sinkholes And The Engineering And Environmental Impacts Of Karst*, pp. 315–326, San Juan, PR, USA, April 2020.

[14] K. L. Garas, M. F. B. Madrigal, R. D. D. Agot, M. C. M. Canlas, and L. S. J. Manzano, "Karst depression detection using IFSAR-DEM: a tool for subsidence hazard assessment in Panglao, Bohol," *Carsologica Sinica*, vol. 39, no. 6, pp. 928–936, 2020.

[15] A. Mihevc and R. Mihevc, "Morphological characteristics and distribution of dolines in Slovenia, a study of a lidar-based doline map of Slovenia," *Acta Carsologica*, vol. 50, no. 1, pp. 11–36, 2021.

[16] R. Ciglič, Š. Čonč, and M. Breg Valjavec, "The impact of digital elevation model preprocessing and detection methods on karst depression mapping in densely forested Dinaric Mountains," *Remote Sensing*, vol. 14, no. 10, p. 2416, 2022.

[17] E. Long, W. M. Chen, F. Xiao, H. H. Liu, J. J. Chen, and L. L. Lang, "Research on extracting plain mountain information using SRTM-DEM and TM data," *Science of Surveying and Mapping*, vol. 2, pp. 53–56, 2008.

[18] L. H. Yan, Z. F. Zhou, D. H. Huang, and Y. S. Dan, "Geomorphic information extraction of karst peak-cluster depression based on Landsat 8," *Science Technology and Engineering*, vol. 18, no. 28, pp. 182–188, 2018.

[19] M. B. Valjavec, M. Zorn, and A. Čarni, "Bioindication of human-induced soil degradation in enclosed karst depressions (dolines) using Ellenberg indicator values (classical karst, Slovenia)," *Science of the Total Environment*, vol. 640-641, pp. 117–126, 2018.

[20] E. Pardo-Igúzquiza, J. J. Durán-Valsero, P. A. Dowd, J. A. Luque-Espinar, J. Heredia, and P. A. Robledo-Ardila, "Geodiversity of closed depressions in a high relief karst: Geoeducation asset and geotourism resource in the "Sierra de las Nieves" National Park (Malaga Province, Southern Spain)," *International Journal of Geoheritage and Parks*, vol. 10, no. 2, pp. 196–217, 2022.

[21] Q. S. Wu, C. B. Deng, and Z. Q. Chen, "Automated delineation of karst sinkholes from lidar-derived digital elevation models," *Geomorphology*, vol. 266, pp. 1–10, 2016.

[22] D. H. Doctor and J. A. Young, "An evaluation of automated GIS tools for delineating karst sinkholes and closed depressions from 1-meter LiDAR-derived digital elevation data, sinkholes and the engineering and environmental impacts of karst," in *Proceedings of the Thirteenth Multidisciplinary Conference on Sinkholes and the Engineering and Environmental Impacts of Karst*, pp. 449–458, New Mexico, 2013.

[23] Y. J. Kim, B. H. Nam, and H. Youn, "Sinkhole detection and characterization using LiDAR-derived DEM with logistic regression," *Remote Sensing*, vol. 11, no. 13, p. 1592, 2019.

[24] G. P. B. Garcia and C. H. Grohmann, "DEM-based geomorphological mapping and landforms characterization of a tropical karst environment in southeastern Brazil," *Journal of South American Earth Sciences*, vol. 93, pp. 14–22, 2019.

[25] V. Zumpano, L. Pisano, and M. Parise, "An integrated framework to identify and analyze karst sinkholes," *Geomorphology*, vol. 332, pp. 213–225, 2019.

[26] X. Xu, *Study on Digital Watershed Analysis Algorithm of Unfilled Sag Grid DEM*, Jiangxi University of Science and Technology, 2016.

[27] J. F. Zhu, T. P. Taylor, J. C. Currens, and M. M. Crawford, "Improved karst sinkhole mapping in Kentucky using lidar techniques: a pilot study in floyds," *Journal of Cave and Karst Studies*, vol. 76, no. 3, pp. 207–216, 2014.

[28] D. G. Tarboton, R. L. Bras, and I. Rodriguez-Iturbe, "On the extraction of channel networks from digital elevation data," *Hydrological Processes*, vol. 5, no. 1, pp. 81–100, 1991.

[29] N. Huang and X. Yang, "Saddle point extraction method based on contour spatial relation," *Geo-Information Science*, vol. 22, no. 3, pp. 410–421, 2020.

[30] X. Meng, L. Y. Xiong, X. W. Yang, B. S. Yang, and G. A. Tang, "A terrain openness index for the extraction of karst Fenglin and Fengcong landform units from DEMs," *Journal of Mountain Science*, vol. 15, no. 4, pp. 752–764, 2018.

[31] X. W. Yang, G. A. Tang, X. Meng, and L. Y. Xiong, "Saddle position-based method for extraction of depressions in Fengcong areas by using digital elevation models," *ISPRS International Journal of Geo-Information*, vol. 7, no. 4, p. 136, 2018.

[32] X. Yang, G. Tang, X. Meng, and L. Xiong, "Classification of karst Fenglin and Fengcong landform units based on spatial relations of terrain feature points from DEMs," *Remote Sensing*, vol. 11, no. 16, p. 1950, 2019.

[33] S. J. Wang, Q. S. Wu, and D. Ward, "Automated delineation and characterization of drumlins using a localized contour tree approach," *International Journal of Applied Earth Observation and Geoinformation*, vol. 62, pp. 144–156, 2017.

[34] Q. S. Wu, H. X. Liu, S. J. Wang, B. L. Yu, R. Beck, and K. Hinkel, "A localized contour tree method for deriving geometric and topological properties of complex surface depressions based on high-resolution topographical data," *International Journal of Geographical Information Science*, vol. 29, no. 12, pp. 2041–2060, 2019.

[35] Q. S. Wu and C. R. Lane, "Delineation and quantification of wetland depressions in the prairie pothole region of North Dakota," *Wetlands*, vol. 36, no. 2, pp. 215–227, 2016.

[36] F. Y. Liang and B. Xu, "Discrimination of tower-, cockpit-, and non-karst landforms in Guilin, southern China, based on morphometric characteristics," *Geomorphology*, vol. 204, pp. 42–48, 2014.

[37] X. Meng, *Extraction and Morphological Characteristics Analysis of Karst Depression in Peak Cluster Area Based on DEM*, Nanjing Normal University, 2019.

[38] E. Pardo-Igúzquiza and P. A. Dowd, "The mapping of closed depressions and its contribution to the geodiversity inventory," *International Journal of Geoheritage and Parks*, vol. 9, no. 4, pp. 480–495, 2021.

[39] S. Čonč, T. Oliveira, R. Portas, R. Cerne, M. B. Valjavec, and M. Krofel, "Dolines and cats: remote detection of karst depressions and their application to study wild felid ecology," *Remote Sensing*, vol. 14, no. 3, p. 656, 2022.

[40] S. A. Berezinskii, A. V. Egorov, V. S. Lashmanova, and I. A. Polinkovskii, "Design of penstocks of pumped-storage stations," *Hydrotechnical Construction*, vol. 19, no. 4, pp. 180–187, 1985.

[41] J. Hartmanis, "Computers and intractability: a guide to the theory of np-completeness (MichaelR. Garey and Davids. Johnson)," *SIAM Review*, vol. 24, no. 1, pp. 90-91, 1982.

[42] P. Padey, R. Girard, D. Le Boulch, and I. Blanc, "From LCAs to simplified models: a generic methodology applied to wind power electricity," *Environmental Science & Technology*, vol. 47, no. 3, pp. 1231–1238, 2013.

[43] Y. J. Kim, B. H. Nam, Y.-H. Jung et al., "Probabilistic spatial susceptibility modeling of carbonate karst sinkhole," *Engineering Geology*, vol. 306, article 106728, 2022.

[44] P. L. Valle, "Karst depression morphology in south Central Kentucky," *Geografiska Annaler: Series A, Physical Geography*, vol. 50, no. 2, pp. 94–108, 1968.

[45] W. P. Williams, "Illustrating morphometric analysis of karst with examples from New Guinea," *Zeitschrift für Geomorphologie*, vol. 15, pp. 40–61, 1971.

[46] M. Day, "Doline morphology and development in Barbados," *Annals of the American Association of Geographers*, vol. 73, no. 2, pp. 206–219, 1983.

[47] C. Denizman, "Morphometric and spatial distribution prarmeters of karstic depressions, lower Suwannee River basin, Florida," *Journal of Cave and Karst Studies*, vol. 61, no. 1, pp. 29–35, 2003.

[48] S. Magdalene and E. C. Alexander, "Sinkhole distribution in Winona County, Minnesota revisited," in *Karst geohazards*, pp. 43–51, Rotterdam, Balkema, 1995.

[49] H. Chen, T. Oguchi, and P. Wu, "A semi-automatic model for sinkhole identification in a karst area of Zhijin County, China," in *International Conference on Intelligent Earth Observing and Applications (IEOAs)*, pp. 209–216, Guilin, 2015.

[50] X. W. Yang, *Study of Topographic Characteristics and Spatial Differentiation of Karst Forest Peaks Based on DEM*, Nanjing Normal University, 2019.

[51] E. Pardo-Iguzquiza, J. J. Duran, and P. A. Dowd, "Automatic detection and delineation of karst terrain depressions and its application in geomorphological mapping and morphometric analysis," *Acta Carsologica*, vol. 42, no. 1, pp. 17–24, 2013.

[52] M. Z. Öztürk, "Morphometric analyses of karstic depressions (dolines)," *Coğrafya Dergisi*, vol. 36, pp. 1–13, 2018.

[53] E. Šegina, Č. Benac, J. Rubinić, and M. Knez, "Morphometric analyses of dolines—the problem of delineation and calculation of basic parameters," *Acta Carsologica*, vol. 47, no. 1, 2018.

[54] A. Basso, E. Bruno, M. Parise, and M. Pepe, "Morphometric analysis of sinkholes in a karst coastal area of southern Apulia (Italy)," *Environmental Earth Sciences*, vol. 70, no. 6, pp. 2545–2559, 2013.

[55] T.-W. Barbara, "Detection of karst features in the Black Hills area in South Dakota/Wyoming, USA, based on evaluations of remote sensing data," *Geosciences*, vol. 8, no. 6, p. 192, 2018.

[56] J. Qureshi, S. A. Mahmood, A. Masood, P. Khalid, and I. S. Kaukab, "DEM and GIS-based hypsometric analysis to study tectonics and lithologies in southern Suleiman fold and thrust belt (Balochistan–Pakistan)," *Arabian Journal of Geosciences*, vol. 12, no. 5, pp. 1–15, 2019.

[57] J. J. Wu, S. W. Chen, K. X. Zheng et al., "Monitoring methodology study of a reservoir built on the karst depression: a large scale laboratory simulation test," *ACS Omega*, vol. 8, no. 16, pp. 14520–14530, 2023.

[58] Y. N. Yang, X. Mo, L. M. Zhong, Q. Zhang, X. B. Kang, and B. Y. Mao, "Karstic conduits and watershed identification based on the morphological characteristics of depressions in the Yunnan–Guizhou Plateau of China," *Environmental Earth Sciences*, vol. 79, no. 1, pp. 1–12, 2020.

[59] P. Chen, F. S. Sun, B. Zhang, and Z. H. Guo, "A new algorithm for DEM low depression treatment in hydrological model," *China Rural Water and Hydropower*, vol. 5, pp. 28–41, 2014.

[60] P. P. Guo, C. M. Li, Y. Yin, and S. T. Ding, "Research on contour tree building algorithm based on adjacency relation," *Chinese Engineering Science*, vol. 15, no. 5, pp. 42–46, 2013.

[61] F. Šušteršič, "A conceptual model of Dinaric solution doline dynamics," *Cave and Karst Science*, vol. 44, no. 2, pp. 66–75, 2017.

[62] Z. Ding, X. Gao, Y. H. Li, and X. Y. Yu, "Regional characteristics and resource-environmental effects of karst depressions in Shilin county, China," *Mountain Research*, vol. 37, no. 3, pp. 316–327, 2019.

[63] J. Chen, S. T. Yang, H. W. Li, B. Zhang, and J. R. Lv, "Research on geographical environment unit division based on the method of natural breaks (Jenks)," *The International Archives of the Photogrammetry, Remote Sensing and Spatial Information Sciences*, vol. XL-4/W3, pp. 47–50, 2013.

[64] J. Zhu, A. M. Nolte, N. Jacobs, and M. Ye, "Using machine learning to identify karst sinkholes from LiDAR-derived topographic depressions in the bluegrass region of Kentucky," *Journal of Hydrology*, vol. 588, article 125049, 2020.

[65] J. W. Xu, S. M. Fang, and R. H. Huang, "A study of spatial morphological characteristics and genesis of peak-cluster depressions of the Qibailong National Geopark in Guangxi," *Acta Geoscientia Sinica*, vol. 38, no. 6, pp. 961–970, 2017.

[66] S. Y. Hong, X. H. Shen, F. Jing, and Z. C. Du, "An analysis of geomorphology characteristics of the Altal Mountain based on DEM," *Remote Sensing for Land & Resources*, vol. 3, pp. 62–66, 2007.

[67] F. F. Gao, H. Liu, and J. W. Deng, "Analysis on geological genesis of karst depression in Guizhou province," *Subgrade Engineering*, vol. 165, no. 6, pp. 23–26, 2012.

[68] X. Miao, X. Qiu, S. S. Wu, D. Gouzie, and H. J. Xie, "Developing efficient procedures for automated sinkhole extraction from lidar DEMs," *Photogrammetric Engineering & Remote Sensing*, vol. 79, no. 6, pp. 545–554, 2013.

[69] M. Shaw-Faulkner, K. Stafford, and A. Bryant, "Delineation and classification of karst depressions using LiDAR: fort hood military installation, Texas," in *In Full Proceedings of the Thirteenth Multidisciplinary Conference on Sinkholes and the Engineering and Environmental Impacts of Karst*, pp. 459–467, New Mexico, 2013.

[70] F. Gutiérrez, M. Parise, J. DeWaele, and H. Jourde, "A review on natural and human-induced geohazards and impacts in karst," *Earth-Science Reviews*, vol. 138, pp. 61–88, 2014.

[71] W. Huang, C. Deng, and J. M. Day, "Differentiating tower karst (fenglin) and cockpit karst (fengcong) using DEM contour, slope, and centroid," *Environmental Earth Sciences*, vol. 72, pp. 407–416, 2013.